ARTICLE

Quantifying Co-Oligomer Formation by α-Synuclein

Marija Iljina,[‖,†,⊥] Alexander J. Dear,[‖,†,§] Gonzalo A. Garcia,[†] Suman De,[†] Laura Tosatto,[†,#] Patrick Flagmeier,[†,§] Daniel R. Whiten,[†] Thomas C. T. Michaels,[†] Daan Frenkel,[†] Christopher M. Dobson,[†,§] Tuomas P. J. Knowles,*[,†,§] and David Klenerman*[,†,‡]

†Department of Chemistry, University of Cambridge, Lensfield Road, Cambridge CB2 1EW, United Kingdom
‡UK Dementia Research Institute, University of Cambridge, Cambridge CB2 0XY, United Kingdom
§Department of Chemistry, Centre for Misfolding Diseases, Lensfield Road, Cambridge CB2 1EW, United Kingdom

Ⓢ *Supporting Information*

ABSTRACT: Small oligomers of the protein α-synuclein (αS) are highly cytotoxic species associated with Parkinson's disease (PD). In addition, αS can form co-aggregates with its mutational variants and with other proteins such as amyloid-β (Aβ) and tau, which are implicated in Alzheimer's disease. The processes of self-oligomerization and co-oligomerization of αS are, however, challenging to study quantitatively. Here, we have utilized single-molecule techniques to measure the equilibrium populations of oligomers formed *in vitro* by mixtures of wild-type αS with its mutational variants and with Aβ40, Aβ42, and a fragment of tau. Using a statistical mechanical model, we find that co-oligomer formation is generally more favorable than self-oligomer formation at equilibrium. Furthermore, self-oligomers more potently disrupt lipid membranes than do co-oligomers. However, this difference is sometimes outweighed by the greater formation propensity of co-oligomers when multiple proteins coexist. Our results suggest that co-oligomer formation may be important in PD and related neurodegenerative diseases.

KEYWORDS: *single-molecule fluorescence, statistical mechanical modeling, cross-aggregation, mixed oligomers, oligomer toxicity, neurodegeneration*
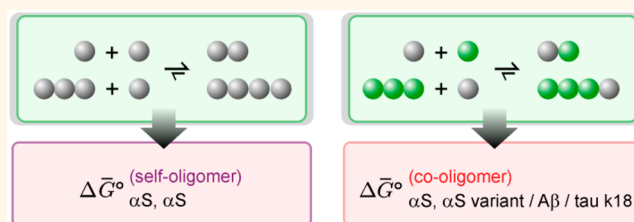
The aggregation of the protein α-synuclein (αS) from its soluble monomeric form into amyloid fibrils is associated with a range of devastating neurodegenerative disorders such as Parkinson's disease (PD) and a series of related synucleinopathies.[1] In these conditions, amyloid fibrils of αS are segregated into cytoplasmic brain inclusions, Lewy bodies, or Lewy neurites,[2] although molecular complexes consisting of a small number of αS monomers, termed oligomers, are increasingly recognized as the most-cytotoxic forms, giving rise to the disease etiology.[3−7] It has also been found that single-residue mutational variants of the protein, including A30P, E46K, and A53T, are associated with familial forms of PD.[8−10] Moreover, aggregates of αS are observed in more than half of the patients suffering from Alzheimer's disease (AD) along with the more-characteristic deposits of the amyloid-β (Aβ) peptide and the protein tau.[11] The co-occurrence of the aggregates of αS, Aβ, and tau has been reported in a variety of neurodegenerative conditions, and it has been suggested that this enhancement could be due to co-interactions between the proteins.[12]

αS has been shown *in vitro* to assemble into a large variety of oligomers with distinct morphologies, structures, and func-

tional properties. Such oligomers can be formed via different mechanisms and include non-fibrillar off-pathway species and prefibrillar intermediates of the amyloid fibril formation process.[7,13−16] The mutational variants of αS have been found to affect the rates of αS aggregation[17−19] and oligomer formation[20] and to alter its interactions with lipid membranes.[21] The effects of the amino acid substitutions on the rate of oligomer formation and the number of oligomers remain unclear. Previous studies have reported either increased[4,18,22] or unaltered[20] levels of oligomers formed by the mutational variants relative to wild-type αS. Additionally, the formation of co-oligomers between different variants of αS has been observed to occur in aqueous solution.[23]

In addition to its ability to self-assemble into a variety of oligomeric species, αS has been reported to interact with other proteins, including Aβ and tau. For example, the effects of αS and Aβ cointeraction on the aggregation of Aβ42 *in vitro* have
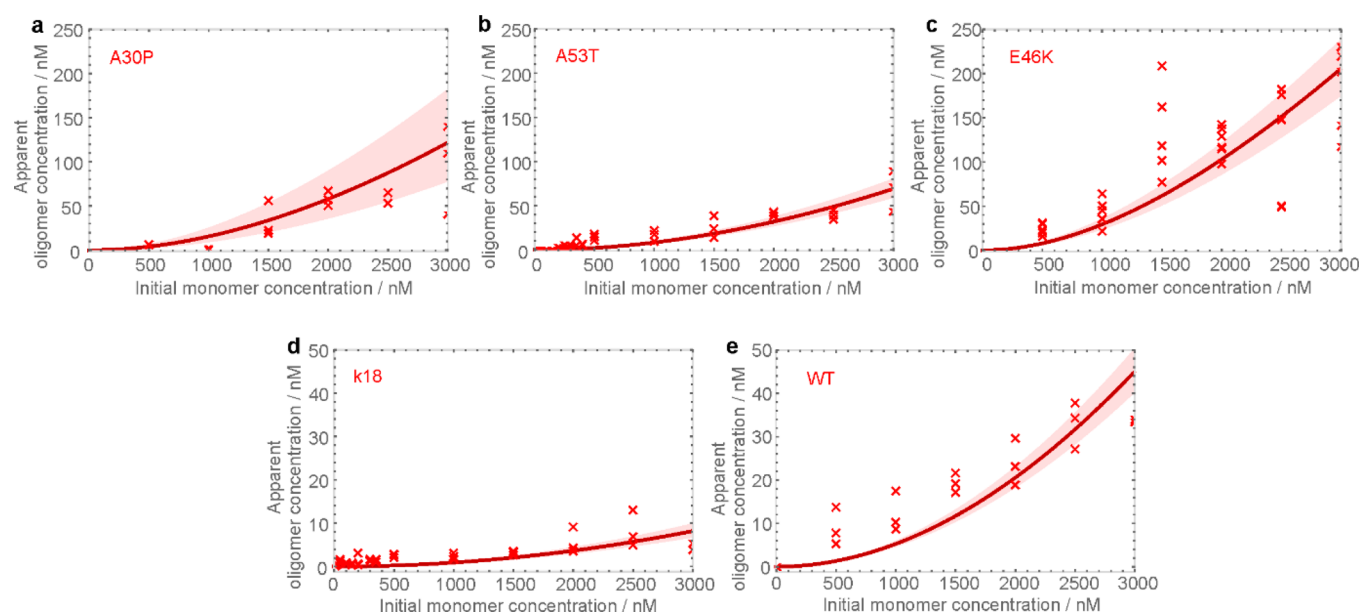
Figure 1. Equilibrium populations of self-oligomers plotted against the total initial protein concentrations. A total of three to five separate samples were analyzed for each initial concentration of monomeric protein. The resulting values are represented by red crosses, and the fit to a single-peptide oligomerization model is shown as a solid line. The shaded bounds represent the fitting error derived using nonparametric bootstrapping, as detailed in the Methods section.

recently been delineated,[24] and the direct binding between αS and Aβ40 and Aβ42 in solution has been characterized[25−27] as well as the direct interaction of αS and tau.[28−30] The formation of co-oligomers containing both αS and Aβ has been predicted by several molecular dynamics simulations.[31−33] Furthermore, the formation of a dimer composed of αS and Aβ domains upon their coordination to Cu^{2+} has been reported,[34] and the formation of co-oligomers of αS and tau has been observed *in vitro*.[35] The accumulation of co-oligomers of αS and tau in the human brain has been shown using novel conformational-specific antibodies.[36] In addition, the formation of co-oligomers of αS with Aβ and tau in human red blood cells has recently been reported.[37]

Despite the accumulating evidence that αS can form self-oligomers as well as co-oligomers with other proteins, the extent of formation and the properties of these co-oligomeric species remain to be determined and quantified. Most *in vitro* investigations, particularly at low physiologically relevant protein concentrations, have focused on the self-oligomerization of αS because its co-oligomerization is difficult to detect and quantify under these conditions. A comprehensive characterization of the self-oligomerization process of αS and its co-oligomerization with the mutational variants or Aβ and with tau can help to compare their relative abundances, and functional assays can reveal the relative cytotoxicities of the self- and co-oligomeric species. To address these issues, we have combined the highly sensitive single-molecule two-color coincidence detection (sm-TCCD) technique,[38] which enables the selective detection of both self- or co-oligomeric species, with statistical mechanical modeling.[39] Using these methodologies, we have characterized the self-oligomerization of wild-type αS; its co-oligomerization with the mutational variants A30P, A53T, and E46K; and its co-oligomerization with Aβ40 and Aβ42 and tau construct k18, which contains four repeats of the aggregation-prone region of full-length tau,[40] at physiologically relevant protein concentrations in aqueous solution. We have derived the equilibrium free energies of

oligomer formation for the studied protein combinations, enabling a quantitative comparison of the self- and co-oligomerization processes. Furthermore, we have investigated the ability of the characterized self- and co-oligomers to permeabilize lipid vesicles, allowing us to quantify and compare their potential for lipid membrane disruption.

RESULTS AND DISCUSSION

TCCD Measurements of the Formation of Self-Oligomers. We first performed sm-TCCD measurements of self-oligomer formation by wild-type αS (subsequently abbreviated as "WT"), A30P, A53T, and E46K αS using singly labeled monomers bearing Alexa Fluor 488 (AF488) and Alexa Fluor 594 (AF594) fluorophores. These fluorescent labels were incorporated at residue 90 of αS molecules, which has been shown not to perturb its aggregation propensity in our previous work.[7] In the experiments, samples containing a 1:1 stoichiometric ratio of AF488 and AF594-labeled monomers of the same protein were combined over a wide range of initial total protein concentrations ranging from low-nanomolar concentrations to 3 μM, corresponding to the reported range of the physiological abundance of αS.[41−43] Solutions were incubated under quiescent conditions for 72 h at 37 °C in a buffer of physiological pH and ionic strength (defined in the Methods section) to generate equilibrium populations of oligomers. Such quiescent conditions have been previously shown to generate αS oligomers but not fibrils.[15,44,45] Note, however, that no oligomer enrichment steps are employed in our preparation in contrast to previously reported protocols.[15] Indeed, the absence of fibril formation under these incubation conditions was confirmed by transmission electron microscopy (TEM) (see the Supporting Information). Furthermore, it was verified that incubation for 72 h is sufficient to generate equilibrium populations of oligomers, even for the A30P isoform, which is characterized by the slowest aggregation kinetics[20,21] (Figure S2). In addition to αS, we also analyzed the self-oligomerization of the Alexa Fluor (AF)-labeled
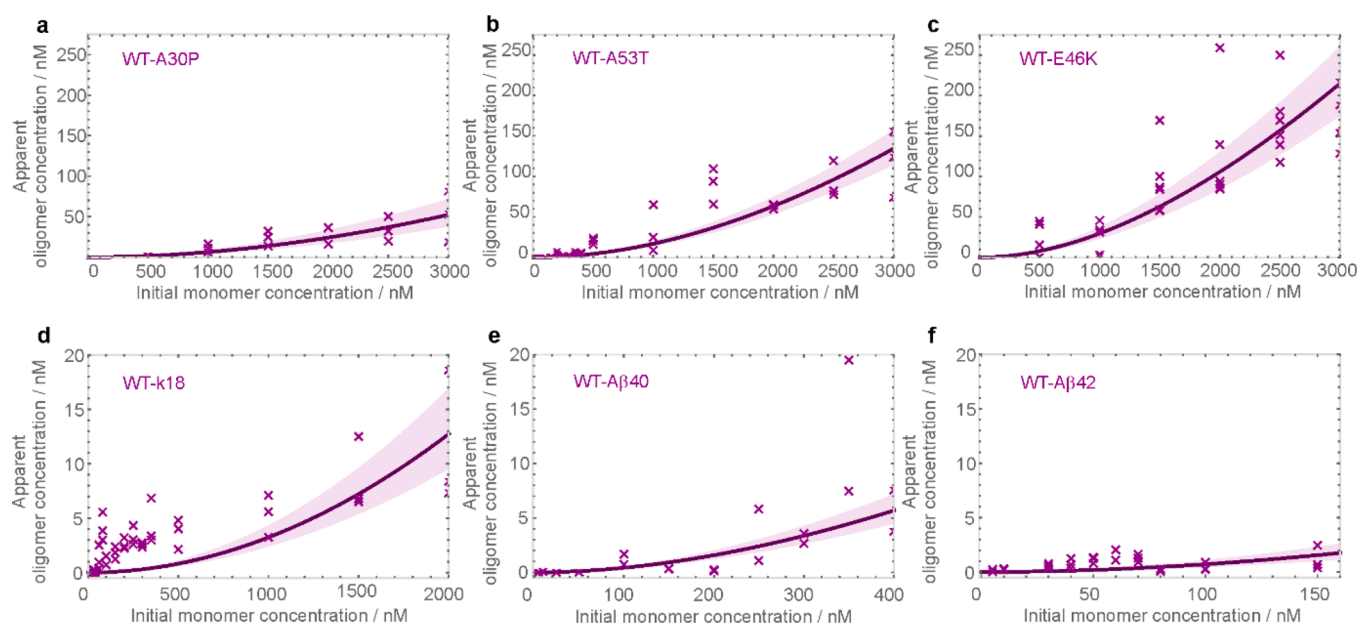
Figure 2. Equilibrium populations of co-oligomers formed in 1:1 mixtures of the various protein combinations as indicated in the panels. A total of two to five separate samples were studied at each concentration. Individual values are represented as purple crosses, and the fit to a two-peptide model of oligomer formation is denoted by a solid line. The shaded bounds represent the fitting error, as in Figure 1. Note that the apparent low oligomer concentrations in panels e and f are due to the lower monomer concentration ranges investigated (see the *x* axes). In fact, these concentrations are predicted to be higher than for other co-oligomers over the same monomer concentration range.

construct of tau protein k18, which comprises the central region of this protein that is included in the microtubule binding region and is frequently used to study tau aggregation.[46,47] For the experiments with k18, the same concentrations and incubation conditions were used as with αS isoforms to enable a direct comparison of the oligomerization potential of both proteins.

During the incubation of protein solutions containing 1:1 ratios of AF488- and AF594-labeled monomers of αS and of the tau construct, the oligomers containing both fluorescent dyes were formed and were quantified by sm-TCCD.[38] For the sm-TCCD measurement, the withdrawn protein solutions were immediately diluted to pM concentrations to enable single-molecule analysis, and continuously passed through a microfluidic device mounted on a single-molecule fluorescence microscope to reduce the detection time, as previously detailed.[48] We previously verified that oligomers remained stable during single-molecule measurements under the same conditions.[49] The solutions were excited by overlapped and focused 488 and 594 nm laser beams, and fluorescence bursts from AF488 and AF594 were simultaneously detected in the two separate emission channels. Thus, AF488-labeled molecules gave rise to discrete noncoincident fluorescence bursts in the AF488 channel, while AF594-labeled molecules lead to fluorescence bursts in the AF594 channel. Any fluorescence bursts that were coincident in both channels corresponded to the oligomers bearing both AF488 and AF594. These dual-labeled species were distinguished from the excess of singly labeled species and quantified by the criterion of temporal coincidence according to eq 1 (see the Methods section). Note that this approach allows the selective monitoring and quantification of only the dual-labeled oligomer species and not singly labeled species, and we therefore refer to the resulting oligomer concentrations as "apparent oligomer concentrations". In addition, the characterization of their exact physical sizes or structures is beyond the scope of this

technique. We confirmed the absence of any direct interactions between the free AF dyes used in our experiments by doing control experiments using free AF488 and AF594 in aqueous buffer, as described in the Supporting Information and Figure S2. The resulting plots of the apparent concentrations of self-oligomers of αS A30P, A53T, E46K, and WT and of tau k18 are shown in Figure 1a−e. The data show that the oligomer populations formed under these conditions are below 200 nM, highlighting the challenge of studying these species by less sensitive bulk experimental techniques. The oligomer populations of the αS variants A30P, A53T, and E46K reached higher levels than the WT protein, with E46K giving the highest apparent oligomer concentrations. The highest apparent equilibrium concentrations of oligomers were observed at the highest total starting αS concentrations, as expected by mass action, in agreement with our previous study of oligomer formation by αS.[49] The apparent concentrations of oligomers formed by k18 were mostly below 10 nM, which is consistent with the expected low aggregation propensity of this protein in aqueous buffer solution in the absence of aggregation inducers.[46,47] They were nevertheless sufficiently above the background, confirming the formation of a low population of oligomeric species under the incubation conditions used here (Figure S2).

TCCD Measurements of the Formation of Co-Oligomers. We next set out to determine whether or not αS WT could co-oligomerize with its mutational variants, as well as with Aβ40, Aβ42, and k18, by combining equimolar ratios of the WT with the other proteins. The 1:1 mixtures of αS WT with its mutational variants are likely to be physiologically relevant as the variants of αS are known to coexist with αS WT *in vivo*.[8−10] The interactions of αS with Aβ40 and with Aβ42, both of which are largely extracellular, is of interest in the light of the reported role extracellular αS may play in neurodegeneration.[50] The potential co-interaction of αS WT with the tau construct k18 is of interest because both
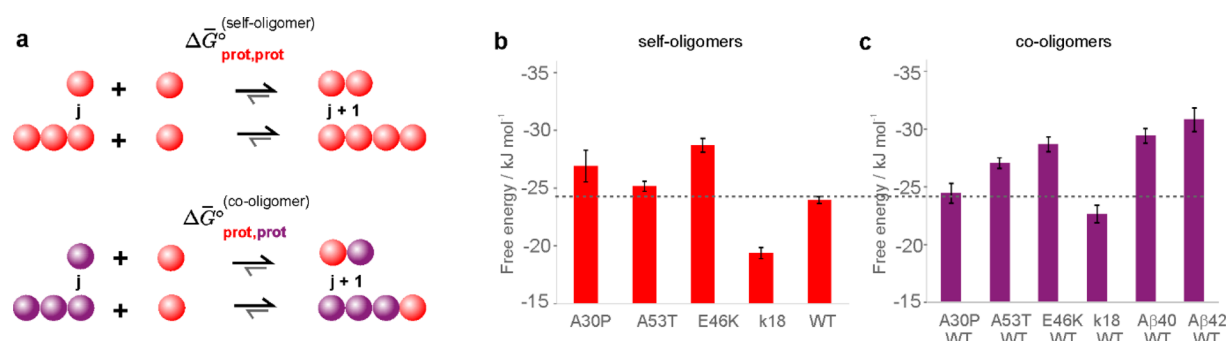
Figure 3. Modeling of self- and co-oligomer formation. (a) Schematic representation of the two processes. The fitted values of free energies of oligomerization, $\Delta G°$ values, derived from the analysis of sm-TCCD data for the formation (b) of self-oligomers and (c) of co-oligomers. The standard errors in the $\Delta G°$ values were determined using a non-parametric bootstrap approach as defined in the Methods section. The dotted line denotes the $\Delta G°$ for the formation of oligomers from WT.

αS and tau proteins are predominantly intracellular and, therefore, are likely to coexist under the same conditions.

To quantify the extent of co-oligomerization of the various protein combinations, we combined and incubated 1:1 stoichiometric ratios of αS WT, singly labeled with AF488, with each of these other proteins, singly labeled with AF594, and selectively monitored the formation of co-oligomeric species that contain both fluorophore labels by sm-TCCD following the same protocols, as described above for the detection of self-oligomers. The apparent oligomer concentrations measured in this way are shown in Figure 2, indicating that co-oligomeric species are formed with all of the protein combinations. The apparent equilibrium concentrations of co-oligomers of αS WT and A30P (Figure 2a) can be seen to be similar to the apparent concentrations of self-oligomers of αS WT (Figure 1e). Interestingly, the apparent concentrations of αS WT co-oligomers with A53T and E46K (Figure 2b,c) are similar to the apparent concentrations of oligomers generated by the mutational variants alone (Figure 1b,c), and are higher than the apparent concentrations of the self-oligomers of αS WT (Figure 1e). Our observation that αS WT can readily co-oligomerize with all of the chosen mutational variants differs from the conclusion of a relatively recent single-molecule study that identified selectivity in the co-interactions with these different mutants.[23] The experimental conditions in the two studies are, however, different and the incubations were carried out over much longer time scales in the present experiments, thus making the results not directly comparable. The observed populations of co-oligomers between WT and k18 can be seen to be below 20 nM over a similar monomer concentration range (Figure 2d). Despite the low levels of such species, the direct detection of co-oligomerization of αS with tau is interesting, especially considering that there are at least six major isoforms of tau in the human brain.[51] The concentrations of co-oligomers between αS and Aβ detected appear even lower but, in fact, can be predicted to be higher than for all other co-oligomers when comparison is made over the same initial monomer concentration range. This is also an interesting result, especially given that multiple isoforms of Aβ can be present *in vivo*.[52] Indeed, it is likely that various isoforms of tau or of Aβ may also co-assemble because the extent of co-aggregation between different proteins is known to be determined by the identity of their primary sequences.[53]

Theoretical Modeling of Self- and Co-Oligomer Data Sets to Determine the Free Energies of Oligomer formation. We then analyzed the data sets observed for self-

and co-oligomer formation by sm-TCCD (Figures 1 and 2) using a statistical mechanical model similar to a previously reported model.[39] In this theoretical model, the key parameter describing the oligomerization process is the Gibbs free energy of monomer addition to an oligomer or another monomer, $\Delta G°$, independent of oligomer size, as illustrated schematically in Figure 3a. This parameter characterizes the ease of oligomer formation by monomeric species, and the more negative the value, the more favorable the oligomerization.

In the present model, described in detail in the Methods section, the oligomers were treated as simple non-interacting one-dimensional chain structures with nearest-neighbor interactions independent of chain length. The approximation of non-interacting oligomers is reasonable given the very low apparent concentrations of oligomers in the present experiments. For self-oligomers, our model is identical to that previously reported.[39] Note that the modeling explicitly takes into account the fact that only oligomers containing both AF488 and AF594 dyes will be detected, whereas the singly labeled oligomers are not detectable (see the Supporting Information). The modeling of linear co-oligomers requires a substantial new theory to be developed, detailed in the Supporting Information "Co-Oligomer Modeling" section. Under the present conditions, most oligomers are inferred to be dimeric (see the Supporting Information "Oligomer Sizes" section). Therefore, although we cannot rule out the existence of larger nonlinear oligomeric species (*e.g.*, tetrahedral clusters) not explicitly included in our linear oligomer model, they cannot in any case be present at sufficiently high concentrations under the present experimental conditions to significantly affect our analysis. We test this by considering a trimer-only model and a tetramer-only model, finding them to give successively worse fits to the experimental data on self-oligomers (see the Supporting Information "Justifying the Choice of Model" section). Note that dimers are naturally accounted for as the smallest aggregate species in our linear model. We emphasize that oligomers have been shown to have a different structure, stability, and toxicity compared to fibrils;[7,49] thus, our $\Delta G°$ is not the same as for fibril elongation.

Our model is not applicable to the analysis of the data derived for the samples containing Aβ at the highest concentrations investigated because we expect fibrillar aggregates to exist at equilibrium above the critical aggregation concentration for fibril formation, which is the lowest total monomer concentration that is required for the formation of fibrils.[39] Using the same fitting procedure, we previously
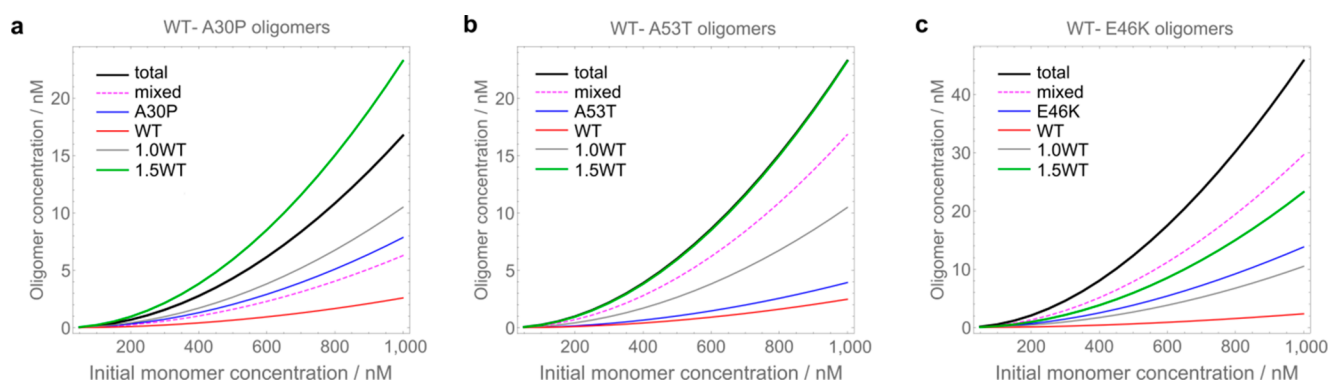
Figure 4. Predicted equilibrium concentrations of protein oligomer populations over the concentration range of 10−1000 nM. In panels a−c, the total concentrations of oligomers generated in 1:1 mixtures of αS WT-mutational variant are shown ("total"), and the separate oligomer subpopulations that are present in these mixtures (co-oligomers are denoted as "mixed", and the self-oligomers of either component as "WT" and the corresponding mutational variant). In addition, αS WT self-oligomers generated at the same total protein concentrations are shown ("1.0WT"), and the oligomers generated at 1.5 times higher total starting concentration of αS WT ("1.5WT"). Note that in panel b, the curves "1.5WT" and "total" overlap.

estimated these critical aggregation concentration values to be 222 ± 10 and 86 ± 10 nM for Aβ40 and Aβ42 isoforms, respectively.[39] Larger fibrillar aggregates were indeed observed using TEM (Figure S1) in solutions containing either Aβ40 or Aβ42 at a 3 μM concentration. Because Aβ comprises only half of the protein molecules in the αS−Aβ solutions, we restricted our analysis of these data sets to total protein concentrations that were up to twice those previously derived critical aggregation concentration values.

Following the fitting of self- and co-oligomer data sets, as detailed in the Methods section, we derived the value of ΔG° of oligomerization of all of the protein combinations investigated in this study. The resulting values, summarized in Figures 3b,c and listed in Table S1, are all large and negative, similar in magnitude to the values previously reported for the formation of Aβ40/42 oligomerizing systems.[39] The least-negative ΔG° value of −19.4 ± 0.5 kJ mol^{-1} was obtained for k18, which is consistent with its lowest propensity to self-assemble under our experimental conditions in the absence of aggregation inducers. Interestingly, the resulting ΔG° value for αS WT of −24.0 ± 0.3 kJmol^{-1} is less negative than the resulting values for all mutational variants of αS except WT-A30P. In addition, the ΔG° values for WT-Aβ co-oligomers (−29.4 ± 0.6 kJmol^{-1} for WT-Aβ40 and −30.8 ± 1.0 kJmol^{-1} for WT-Aβ42) are more negative than the value for αS WT and less negative than our previously obtained values for Aβ40 and Aβ42 self-oligomers (−36.3 kJmol^{-1} for both isoforms).[39] Overall, the more-negative ΔG° values for the mixtures containing the WT protein compared to αS WT alone suggest that the co-oligomer formation by αS WT is more favorable than the self-oligomer formation for most of the mixtures under our experimental conditions.

Predicted Equilibrium Concentrations of Oligomer Populations Based on the Derived Free Energies of Oligomer Formation. The derivation of the free energies of oligomer formation enables the prediction of the total rather than apparent equilibrium concentrations of self- and co-oligomers at any chosen protein concentration. Given that oligomer concentrations depend exponentially on ΔG°s (as detailed in Supporting Information), even slight differences in the derived ΔG° values correspond to large differences in the resulting equilibrium oligomer populations. Indeed, under the present conditions, a stabilization of less than 2 kJ mol^{-1} is

sufficient to result in a doubling of the observed oligomer concentration. To illustrate this statement, we set out to explore the relative concentrations of different types of oligomers formed by the mixtures of αS WT with its mutational variants. To this end, we predicted the overall oligomer concentrations and the concentrations of the separate oligomer subpopulations for the 1:1 mixtures of WT with its variant A30P, A53T, and E46K generated over the total range of protein concentrations from 10 to 1000 nM and compared them with the predicted oligomer populations for αS WT at the same starting protein concentrations. These predictions reveal that the co-oligomers of αS WT-A53T and WT-E46K are the dominant sub-populations across the entire ranges of the protein concentrations (Figure 4). In addition to the concentrations of the self- and co-oligomer sub-populations in the αS WT−mutational variant mixtures, we also predicted the concentrations of oligomers for αS WT at a concentration of αS of 1.5×, which is relevant to the scenario of αS overproduction[54,55] and corresponds to the conditions of its gene duplication.[56] According to these simulations, the total oligomer concentration in the αS WT−mutational variant mixtures can reach similar levels to the 1.5WT system, and even-higher concentrations of oligomers are generated in the case of WT-E46K combination.

Importantly, this analysis shows that the generation of high concentrations of oligomers can be caused not only by the increased concentration of soluble αS WT but also by the presence of the protein variants that have a favorable interaction with the αS WT owing to sequence similarity.[53]

The propensity identified in this study of the mutational variants of αS to generate elevated equilibrium concentrations of oligomers and co-oligomers may explain their pathogenicity, along with other previously established disease-relevant properties of these mutational variants such as perturbed aggregation rates,[17−19] altered binding to lipid membranes,[21,57] and the altered structural organization of the oligomers.[20]

Subsequently, we used the derived ΔG°s to predict the populations of the defined oligomeric species at the protein concentrations that correspond to their physiological abundance, focusing on the mixture of αS WT and Aβ isoforms. Using the protein concentrations that might be present inside a cell, 0.9 and 0.1 nM for Aβ40 and Aβ42, assuming their intracellular concentrations are similar to their extracellular
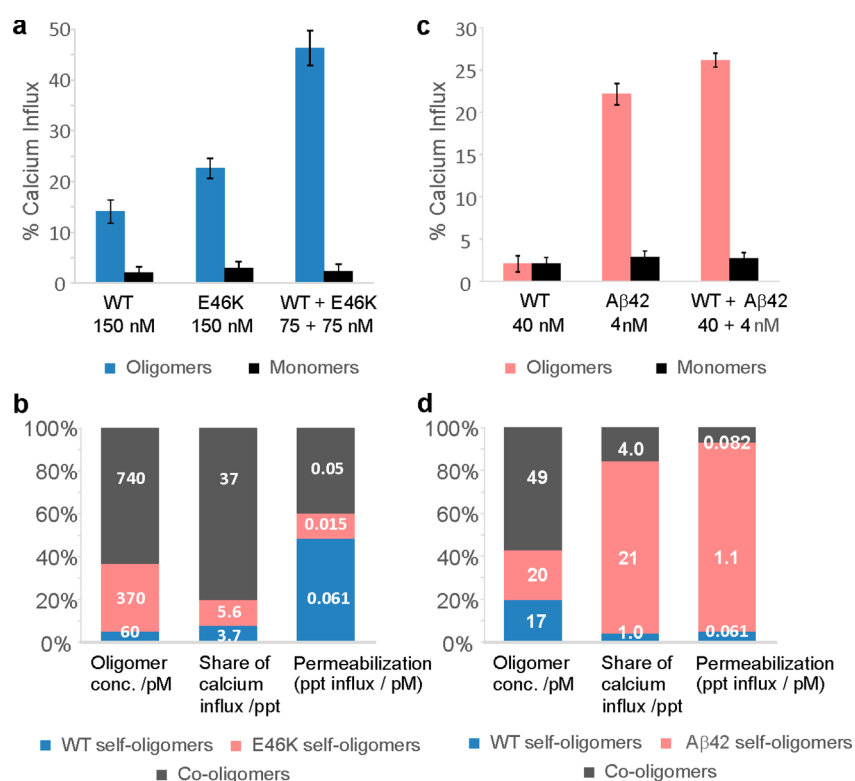
Figure 5. Quantification of the Ca^{2+} influx induced by oligomers using the single vesicle assay. (a) Experimentally measured average values of Ca^{2+} influx, induced by the oligomers formed at equilibrium in solutions containing αS WT and E46K (concentrations in monomer equivalents). Error bars correspond to the standard deviations from three separate experiments for each experimental condition ($p = 0.0495$). (b) Comparing self- and co-oligomer populations to their contributions to total Ca^{2+} influx, and their relative permeabilization propensity, in the αS solution containing both 75 nM WT and 75 nM E46K. (c) Average values of Ca^{2+} influx induced by the oligomers formed at equilibrium in solutions containing αS WT and Aβ42 (concentrations in monomer equivalents). Error bars correspond to the standard deviations from four separate experiments for each experimental condition ($p = 0.0209$). (d) Comparing self- and co-oligomer populations to their contributions to total Ca^{2+} influx, and their relative permeabilization propensity, in the solution containing both αS (40 nM WT) and Aβ42 (4 nM).

concentrations[58] versus 300 nM for αS WT, based on the measured K_d for membrane binding,[59] the major oligomeric form is predicted to be self-oligomers of αS WT (0.96 nM), followed by co-oligomers of αS WT and Aβ (0.05 nM and 0.01 nM for WT-Aβ40 and WT-Aβ42), with Aβ self-oligomers being at concentrations that are orders of magnitude lower. Thus, under these conditions, most of the Aβ peptides within the oligomeric species are incorporated into the co-oligomers with αS WT. At the protein concentrations that correspond to their extracellular abundance in cerebrospinal fluid (CSF), (0.9 and 0.1 nM for Aβ40 and Aβ42 versus 1 nM for αS WT),[41,58] the predicted dominant type of oligomer are self-oligomers of Aβ40 (83%) at a concentration of 1.1 pM. Aβ42-containing oligomers are present at 0.04 pM: 70% of these latter oligomers are predicted to be co-oligomers of αS WT and Aβ42, with 30% being self-oligomers of Aβ42. Remarkably, most of Aβ42 is thus predicted to be a constituent of co-oligomers under these conditions.

Co-Oligomer Formation Leading to Increased Calcium Influx into Lipid Vesicles Due to Membrane Disruption. Next, we set out to examine if the self- and co-oligomers that αS forms with its mutational variants and with the Aβ peptide are able to permeabilize lipid membranes, a process that has been associated with neurotoxicity.[60] We addressed this question by measuring the oligomer-induced permeabilization of lipid membranes using a recently developed ultrasensitive single-vesicle assay that quantifies

Ca^{2+} influx into lipid vesicles upon membrane disruption based on fluorescence-intensity changes of a calcium-sensitive dye.[61] Using this assay and identical experimental conditions, we previously reported that neither monomeric Aβ peptide nor monomeric αS WT cause significant calcium influx;[61] therefore, any influx observed can be attributed to the action of peptide aggregates on the vesicle membranes. The detection of a higher fluorescence intensity corresponds to a larger calcium influx due to a higher level of membrane permeabilization caused by the aggregates.[61] First, we examined the action of αS WT with and without its mutational variant E46K because this combination of αS proteins generated the highest steady-state concentrations of mixed oligomers and was expected to have comparable lipid-binding properties and not to form lipid-induced aggregates under our experimental conditions. Separate solutions of 150 nM monomeric αS WT and of 150 nM monomeric αS E46K variant were prepared and incubated under conditions for which we have characterized the oligomer populations above (Figure 1e,c). We then quantified the ability of these solutions to permeabilize membranes using the single-vesicle assay,[61] by measurement of the total Ca^{2+} influx (Figure 5a). Significant Ca^{2+} influx was observed in both cases, confirming that the self-oligomers formed by these αS variants can disrupt membranes (see the Methods section for further experimental details). We then used our theoretical model to calculate the equilibrium concentration of oligomers formed in each of these solutions

(Table 1). Comparing these figures with the permeabilization data allows us to quantitatively determine the ability of the

Table 1. Predicted Oligomer Concentrations for αS WT-E46K Solutions

αS solution (initial monomer concentrations)	WT self-oligomer concentration (pM)	E46K self-oligomer concentration (pM)	WT-E46K co-oligomer concentration (pM)
WT (150 nM)	240	–	–
E46K (150 nM)	–	1500	–
WT plus E46K (75 plus 75 nM)	60	370	740

respective self-oligomers to induce Ca^{2+} influx [the permeabilization propensity, measured in units of percentage point (ppt) Ca^{2+} influx per picomole].

We next prepared solutions containing both monomeric αS WT and the E46K variant at equimolar concentrations of 75 nM (total concentration of 150 nM) and incubated them under the conditions described above to allow the formation of oligomer populations. We then measured the ability of the solutions containing these oligomer populations to cause Ca^{2+} influx in the vesicle assay (Figure 5a). We again used our theoretical model to determine the concentrations of WT self-oligomers (60 pM), E46K self-oligomers (370 pM), and WT-E46K co-oligomers (740 pM) present in these solutions (Figure 5b). Based on the concentrations of the self-oligomers and their ability to induce Ca^{2+} influx that we have calculated above, we can determine how much of the Ca^{2+} influx of the mixture can be attributed to αS WT self-oligomers (3.7 ppt) and αS E46K self-oligomers (5.6 ppt). The co-oligomers are therefore responsible for 37.1 ppt of the Ca^{2+} influx. Dividing this by the predicted co-oligomer concentration gives us the permeabilization propensity of the WT-E46K co-oligomers.

These results show that although E46K-containing oligomers are formed much more readily than WT oligomers (Table 1), the ability of E46K self-oligomers to cause Ca^{2+} influx is lower compared with the αS WT-containing oligomers, indicated by their lower permeabilization propensity (Figure 5b). The co-oligomers both readily form and significantly disrupt membranes and are thus responsible for the great majority, namely 80%, of the observed Ca^{2+} influx caused by the mixed αS WT-E46K solution (Figure 5b).

Because the toxicity of Aβ42 self-oligomers is also well-established,[61,62] it is of interest to test the potential toxicity of αS WT-Aβ42 co-oligomers. Choosing monomeric concentrations at which co-oligomer formation was predicted to be particularly high, we performed membrane permeabilization experiments (Figure 5c) for solutions containing only self-oligomers (generated from incubation of 4 nM Aβ42 or 40 nM αS WT, respectively) and solutions containing self- and co-oligomers (generated from incubation of 4 nM Aβ42 plus 40 nM αS WT). We employed our theoretical model to calculate the concentrations of αS WT self-oligomers (17 pM), Aβ42 self-oligomers (20 pM), and WT-Aβ42 co-oligomers (49 pM) formed in the mixed solution. Combined with theoretical predictions of the oligomer concentrations formed in the single-species solutions (Table 2), the data enabled us to perform the same analysis as above to determine the relative ability of these different oligomeric species to permeabilize membranes. Our results show that although more than half of the oligomers formed in the mixed solution are co-oligomers,

Table 2. Predicted Oligomer Concentrations for αS WT-Aβ42 Solutions

αS or Aβ solution (initial monomer concentrations)	WT self-oligomer concentration (pM)	Aβ42 self-oligomer concentration (pM)	WT-Aβ42 co-oligomer concentration (pM)
αS WT (40 nM)	17	–	–
Aβ42 (4 nM)	–	21	–
WT plus Aβ42 (40 plus 4 nM)	17	20	49

their contribution to the ability of the solution to permeabilize membranes is small, and therefore, co-oligomers are significantly less disruptive than the self-oligomers (Figure 5d). Interestingly, we also find that Aβ oligomers are over an order of magnitude more disruptive to membranes than αS oligomers and that they are present at similar concentrations (Table 2). The greater number of co-oligomers in this case is insufficient to outweigh the greater membrane permeabilization propensity of Aβ42 self-oligomers, which remain responsible for the majority (80%) of the Ca^{2+} influx caused by the oligomers present in the WT-Aβ42 mixed solutions (Figure 5d).

Because the αS WT protein coexists with its E46K variant in the human brain of subjects displaying a single E46K mutation, which means that the person carries one WT αS allele and one allele with the E46K mutation, species formed during co-aggregation may be involved in membrane permeabilization and the loss of protein homeostasis. Our results show that the presence of E46K mutation leads to the increased formation of E46K self- and co-oligomers and not to these structures being inherently more damaging to lipid membranes. Our results also indicate substantial co-oligomerization between the PD-related αS protein and the AD-associated Aβ42 peptide. However, although this hints at a possible cross-seeding effect that may have relevance for amyloid fibril formation, the co-oligomers themselves appear to be relatively inert in the single-vesicle assay compared with the self-oligomers of Aβ42 and, thus, may have comparatively little direct effect on cell-membrane disruption.

Taken together, our combined experimental and theoretical methodology permits us not only to determine the concentrations of different types of oligomers formed from mixtures of amyloidogenic monomeric peptides and proteins at biologically relevant concentrations but also to gain insight into their likely relative toxicities due to lipid membrane disruption. In addition, the close agreement between the permeabilization propensity values calculated for αS self-oligomers formed from 40 nM and 150 nM monomeric αS solutions (Figure 5b,d) clearly demonstrates the self-consistency of our modeling approach. The number of possible cytotoxic αS-containing co-oligomer types can, in principle, be very large in vivo, considering that new αS mutational variants are still being discovered[63,64] and numerous post-translationally modified and truncated proteoforms of αS are physiologically abundant,[65] as well as multiple isoforms of Aβ[66] and other amyloidogenic proteins and their complexes.[67] More generally, most proteins associated with neurodegenerative diseases are found to be post-translationally modified in the aggregated state so that the formation of co-oligomers, either between different post-translationally modified forms of the same protein or different proteins present in the same cellular

compartment, is likely to play a much more important role in neurodegenerative diseases than previously thought.

CONCLUSIONS

In this study, we have performed a detailed quantitative analysis of self- and co-oligomer formation by αS and its mutational variants *in vitro* and investigated its co-oligomerization with two major AD-related proteins, Aβ and tau k18 construct. We have compared the potential for lipid membrane disruption by the different oligomer types using a single-vesicle assay. Our results show that at low physiologically relevant protein concentrations, co-oligomer formation in most cases is more favorable than self-oligomer formation by αS, and thus, αS-containing co-oligomers may be highly abundant under conditions in which multiple proteins coexist. We also find that although the co-oligomers examined are less potent membrane disruptors in comparison to self-oligomers, their adverse effects can become dominant when the co-oligomers are present at high steady-state concentrations. The identified favorable formation of co-oligomers between αS and other proteins and the high potential of the resulting species to disrupt lipid membranes are important in the context of synucleinopathies and in the development of therapeutics against the onset and progression of these diseases.

METHODS

Preparation of Self- and Co-Oligomer Samples. Monomeric αS with an alanine to cysteine mutation, WT αS-A90C, A30P-A90C, A53T-A90C, and E46K-A90C were expressed and purified based on the protocol by Hoyer et al.[68] and stored at −80 °C with the addition of dithiothreitol. Fluorescent labeling at residue 90 was carried out using Alexa Fluor (AF) 488 and 594 dyes (maleimide linkers, Invitrogen Lifesciences) according to previously reported protocols[7,20,49] by incubating the protein with 1.5 molar excess of the AF dyes overnight at 4 °C in degassed phosphate-buffered saline (PBS) buffer (10 mM phosphate, 0.27 mM KCl and 137 mM NaCl at pH 7.4) and subsequent separation of the unreacted dyes on PD10 columns (GE Healthcare). The labeling efficiency was checked by mass spectrometry and the samples with labeling efficiency above 95% were selected (see the Supporting Information for representative spectra). The expression and purification of k18 tau was performed as previously reported,[69] and labeling with the AF dyes was carried out as for αS.[7,20,49] Monomeric solutions of HiLyteFluor 488 (Anaspec, Fremont) were prepared as described previously[62,70] by dissolving the lyophilized peptide in NaOH at pH 12, sonicating over ice for 15 min (Bandelin Sonorex), and flash-freezing into aliquots and storing at −80 °C. For the incubations, 1:1 molar ratios of 488- and 594-labeled protein monomers were combined in PBS buffer (composition defined above) up to the final volume of 900 μL, and the protein combinations are shown in Figures 1 and 2. Note that in the co-oligomerization experiments, a 1:1 molar ratio of AF488-labeled protein variant is combined with a different protein variant that is labeled with AF594, and thus, the species that contain both AF488 and AF594 correspond to the co-assemblies between the two protein variants and the self-oligomers of either protein are not monitored. A total of three separate samples for each concentration (in the range of 0−3 μM of total protein) and protein combination were prepared. LoBind microcentrifuge test-tubes (Eppendorf, Hamburg, Germany) were used for all incubations to prevent surface absorption, as had been found to be effective in previous studies.[20,48,49,71] Incubations were performed for 3 days at 37 °C without agitation. Upon withdrawal, the solutions were rapidly diluted to 100 pM concentrations to enable single-molecule analysis and subsequently analyzed using sm-TCCD.

TCCD Measurements and Data Analysis. TCCD measurements were performed using a custom-built single-molecule fluorescence microscope as previously described,[49,69] utilizing fast-flow microfluidics for sample detection[48] and closely following previously reported protocols.[39] Dual-laser beam excitation was used by exciting the solutions to be analyzed with collimated and overlapped 488 nm (Spectra Physics NewPort Cyan) and 594 nm (Cobolt Lasers) laser beams operating at 2 and 1.3 mW powers (measured at the back port of the microscope), reflected by a dichroic mirror (Semrock DiO1 R405/488/594), and sent through an oil immersion objective (Plan Apo VC 60×, NA 1.40, Nikon) to be focused 10 μm into the center of a microfluidic channel. The two laser foci were visualized using a CCD camera and overlapped by manually adjusting their shapes and positions in the xy plane. The laser beam overlap was routinely checked by a stationary measurement using a dual-labeled (with 1:1 AF488 and AF594) 40-bp TCCD DNA duplex at 25 pM concentration following previously published procedures,[48] and the alignment was regularly carried out prior to protein measurements to ensure maximum beam overlap. Fluorescence signal was collected by the same objective, imaged onto a 100 μm pinhole (Thorlabs), and separated into two channels by a dichroic mirror (Horiba 585DRLP). The pinhole was conjugate with the plane of focus of the microscope objective and the point of the laser excitation and, thus, eliminated out-of-focus fluorescence and scattered light and reduced the background noise. Donor fluorescence was filtered by a long-pass (Edge Basic 514) and a band-pass filter (535AF45 Omega Filters) before being focused onto an avalanche photodiode, APD (PerkinElmer). Acceptor fluorescence was directed through a long-pass filter (610ALP Horiba) and a band-pass filter (BrightLine 629/53) before being focused onto a second APD. Synchronous output from the APDs was collected by custom-implemented field-programmable gate array, FPGA (Celoxica RC10). Data were acquired for 600 s (60 frames, 100 000 bins per frame, 100 μs bin-width) per aliquot and consisted of time-binned photon bursts in the donor and the acceptor channel. All measurements were made at ambient temperature around 20 °C.

The collected photon traces were analyzed using custom-written Igor Pro 6.22 (Wavemetrics) software analogous to that previously described.[48] The data were corrected for autofluorescence and for cross-talk. Photon bursts with intensities greater than the threshold of 15 photons per bin in the blue and, in the red channels, were selected according to previously established threshold selection approaches that allowed maximization of the detection of coincident events. Simultaneous events in both channels above the threshold (the AND criterion)[72] were selected. To account for any possible coincident events due to chance, the desynchronization approach was used.[73] Time-bins in the blue channel were randomly renumbered before the selection of simultaneous events in the two channels above the threshold. Using these outputs, the association quotient Q was estimated according to eq 1:

$$Q = \frac{C - E}{A + B - (C - E)} \tag{1}$$

where A is the number of fluorescent bursts in the blue channel, B is the number of fluorescent bursts in the red channel, C is the number of coincident events, and E is the number of chance-coincident events (all above the 15 photons per bin threshold). The apparent oligomer concentrations, presented in Figures 1 and 2, were defined as the fraction of coincident events (oligomers) multiplied by the starting total protein concentration.

Modeling of Self- and Co-Oligomer Data Sets. Having ascertained that the experiments detailed here have reached equilibrium with respect to oligomer formation (Figure S2), we analyzed our results using two equilibrium statistical mechanical models: a previously described single-peptide oligomerization model[39] and a new two-peptide model of co-oligomer formation. The first model considers a solution of a single species of monomeric peptide that can reversibly self-associate to form linear chains of any length. The second model consists of a solution containing two species of monomeric peptide that can reversibly associate to form both mixed- and single-species chains. The equilibrium constants of these reactions can be related to the free energies of monomer

addition to like and unlike peptides or to self- and co-oligomerization. We work in the grand canonical ensemble, and we set the chemical potentials by insisting on conservation of peptide. Furthermore, we consider concentrations not numbers; thus, the only free thermodynamic parameter is the temperature. Thus, the systems described by both models are completely specified by the standard free energies, the peptide concentrations, and the temperature. We can therefore determine the standard free energies by least-squares fitting the apparent oligomer concentrations as a function of initial monomer concentrations.

We first fit the self-oligomer data to the single-species model to obtain the self-oligomerization standard free energies. Note that the model contains a correction factor (calculated exactly analytically) to account for the fact that only the oligomers containing both AF488 and AF594 dye are detected by the experimental measurements, with AF488-only and AF594r-only oligomers being invisible. We then enter these free energies into the two-species model, which we fit to the two-species oligomerization data to determine the co-oligomerization standard free energy. These data only measure the co-oligomer concentration, so we fit only to the mixed oligomer component of the model.

Due to the complicated analytical fitting procedure, a formal parametric approach to error estimation is not suitable. Therefore, we prefer to use a nonparametric bootstrap approach.[74] Our data are effectively stratified by initial monomer concentration; therefore, we also stratify our sampling to better reproduce the structure of the data in our resamples.[75] Furthermore, we prefer a subsampling technique rather than full bootstrap because subsampling is valid under much-weaker conditions than full resampling.[76] Our full method is then to randomly sample one data point at each monomer concentration and fit the resulting subdata set to our model, recording the resultant $\Delta G°$. This process is then repeated many times (we chose to do 500 repeats), generating a distribution of $\Delta G°$. An estimate of the standard error for $\Delta G°$ is then given by the standard deviation of this distribution.

Quantification of Ca²⁺ Influx into Lipid Vesicles. Protein samples were prepared and incubated under the same incubation conditions as for the sm-TCCD assays using unlabeled αS WT, unlabeled E46K, and unlabeled Aβ42 at the total starting protein concentrations as specified in Figure 5. For the detailed description of the preparation of Aβ42 peptide stock and for details on the single-vesicle method, see Flagmeier et al.[61] Briefly, lipid vesicles were composed of 16:0–18:1 PC and 18:1–12:0 biotin PC at a 100:1 ratio and filled with 100 μM Cal-520 in HEPES buffer of pH 6.5. This type of lipids was chosen after testing several different lipid compositions, as detailed before,[61] because it enabled the preparation of a fluid bilayer at room temperature. Even though other lipid compositions can have this property, we avoided using negatively charged lipids due to reported increased binding of E46K mutational variant in comparison to WT αS in their presence.[77,78] Multiple freeze-and-thaw cycles and extrusion using a membrane of 200 nm cutoff were performed. Then, size-exclusion chromatography was carried out to separate non-incorporated dye molecules from the vesicles. Subsequently, the purified vesicles were immobilized onto PLL–PEG coated glass coverslips using a biotin–neutravidin–biotin linkage and incubated in 50 μL Ca²⁺ containing Leibovitz's L-15 solution and were imaged using total internal reflection fluorescence microscopy. Thereafter, 50 μL of protein solution was added, and the same area of the coverslips was imaged to check if the solution induced any influx of Ca²⁺ into the vesicles. Next, ionomycin, an ionophore for cations, was added and incubated for 5 min. Ionomycin allows Ca²⁺ to enter the vesicles and saturates them with Ca²⁺. Subsequently, images of Ca²⁺ saturated single vesicles of the same area were acquired. For each field of view, 50 images were taken with an exposure time of 50 ms. The recorded images were used to determine the fluorescence intensity of each spot under the three different conditions: in the presence of only buffer namely blank (F_{blank}), in the presence of an aggregation mixture (F_{sample}), and after the addition of ionomycin ($F_{Ionomycin}$). The detection of individual spots was implemented using "find maxima", and the intensity of the spots

was calculated by considering a 5 pixel diameter. Finally, the sample-induced relative Ca²⁺ influx into a vesicle was quantified using the following equation:

$$\text{Ca}^{2+} \text{ influx} = \frac{F_{\text{sample}} - F_{\text{blank}}}{F_{\text{ionomycin}} - F_{\text{blank}}} \tag{2}$$

The average degree and standard deviation of Ca²⁺ influx was calculated by averaging the Ca²⁺ influx into individual vesicle from nine fields of view. P values reported in Figure 5 are obtained using a Kruskal–Wallis test with $\alpha = 0.05$. Data from just premixed versus incubated protein samples are compared.

ASSOCIATED CONTENT

Ⓢ Supporting Information

AUTHOR INFORMATION

Corresponding Authors
*E-mail: tpjk2@cam.ac.uk.
*E-mail: dk10012@cam.ac.uk.

ORCID Ⓞ
Marija Iljina: 0000-0002-0824-3707
Patrick Flagmeier: 0000-0002-1204-5340
Tuomas P. J. Knowles: 0000-0002-7879-0140

Present Addresses
⊥Department of Chemical and Biological Physics, Weizmann Institute of Science, POB 26, Rehovot 76100, Israel
#Istituto di Biofisica, Consiglio Nazionale delle Ricerche, via alla Cascata 56/C 38123, Trento, Italy

Author Contributions
∥M.I. and. A.J.D. contributed equally.

Notes
The authors declare no competing financial interest.

ACKNOWLEDGMENTS

REFERENCES

(1) Spillantini, M. G. Parkinson's Disease, Dementia With Lewy Bodies and Multiple System Atrophy Are Alpha-Synucleinopathies. *Parkinsonism Relat. Disord.* **1999**, *5*, 157–162.
(2) Spillantini, M. G.; Schmidt, M. L.; Lee, V. M.; Trojanowski, J. Q.; Jakes, R.; Goedert, M. Alpha-Synuclein in Lewy Bodies. *Nature* **1997**, *388*, 839–840.

(3) Chiti, F.; Dobson, C. M. Protein Misfolding, Functional Amyloid, and Human Disease. *Annu. Rev. Biochem.* **2006**, *75*, 333−366.

(4) Conway, K.; Lee, S.; Rochet, J.; Ding, T.; Williamson, R.; Lansbury, P. Acceleration of Oligomerization, Not Fibrillization, Is a Shared Property of Both Alpha-Synuclein Mutations Linked to Early-Onset Parkinson's Disease: Implications for Pathogenesis and Therapy. *Proc. Natl. Acad. Sci. U. S. A.* **2000**, *97*, 571−576.

(5) Kalia, L. V.; Kalia, S. K.; McLean, P. J.; Lozano, A. M.; Lang, A. E. α-Synuclein Oligomers and Clinical Implications for Parkinson Disease. *Ann. Neurol.* **2013**, *73*, 155−169.

(6) Volles, M. J.; Lee, S. J.; Rochet, J. C.; Shtilerman, M. D.; Ding, T. T.; Kessler, J. C.; Lansbury, P. T. Vesicle Permeabilization by Protofibrillar Alpha-Synuclein: Implications for the Pathogenesis and Treatment of Parkinson's Disease. *Biochemistry* **2001**, *40*, 7812−7819.

(7) Cremades, N.; Cohen, S. I.; Deas, E.; Abramov, A. Y.; Chen, A. Y.; Orte, A.; Sandal, M.; Clarke, R. W.; Dunne, P.; Aprile, F. A.; Bertoncini, C. W.; Wood, N. W.; Knowles, T. P.; Dobson, C. M.; Klenerman, D. Direct Observation of the Interconversion of Normal and Toxic Forms of α-Synuclein. *Cell* **2012**, *149*, 1048−1059.

(8) Polymeropoulos, M. H.; Lavedan, C.; Leroy, E.; Ide, S. E.; Dehejia, A.; Dutra, A.; Pike, B.; Root, H.; Rubenstein, J.; Boyer, R.; Stenroos, E. S.; Chandrasekharappa, S.; Athanassiadou, A.; Papapetropoulos, T.; Johnson, W. G.; Lazzarini, A. M.; Duvoisin, R. C.; Di Iorio, G.; Golbe, L. I.; Nussbaum, R. L. Mutation in the Alpha-Synuclein Gene Identified in Families With Parkinson's Disease. *Science* **1997**, *276*, 2045−2047.

(9) Zarranz, J. J.; Alegre, J.; Gómez-Esteban, J. C.; Lezcano, E.; Ros, R.; Ampuero, I.; Vidal, L.; Hoenicka, J.; Rodriguez, O.; Atarés, B.; Llorens, V.; Tortosa, E. G.; del Ser, T.; Muñoz, D. G.; de Yebenes, J. G. The New Mutation, E46K, of Alpha-Synuclein Causes Parkinson and Lewy Body Dementia. *Ann. Neurol.* **2004**, *55*, 164−173.

(10) Krüger, R.; Kuhn, W.; Müller, T.; Woitalla, D.; Graeber, M.; Kösel, S.; Przuntek, H.; Epplen, J. T.; Schöls, L.; Riess, O. Ala30Pro Mutation in the Gene Encoding Alpha-Synuclein in Parkinson's Disease. *Nat. Genet.* **1998**, *18*, 106−108.

(11) Galpern, W. R.; Lang, A. E. Interface Between Tauopathies and Synucleinopathies: A Tale of Two Proteins. *Ann. Neurol.* **2006**, *59*, 449−458.

(12) Spires-Jones, T. L.; Attems, J.; Thal, D. R. Interactions of Pathological Proteins in Neurodegenerative Diseases. *Acta Neuropathol.* **2017**, *134*, 187−205.

(13) Pieri, L.; Madiona, K.; Melki, R. Structural and Functional Properties of Prefibrillar α-Synuclein Oligomers. *Sci. Rep.* **2016**, *6*, 24526.

(14) Danzer, K. M.; Haasen, D.; Karow, A. R.; Moussaud, S.; Habeck, M.; Giese, A.; Kretzschmar, H.; Hengerer, B.; Kostka, M. Different Species of Alpha-Synuclein Oligomers Induce Calcium Influx and Seeding. *J. Neurosci.* **2007**, *27*, 9220−9232.

(15) Chen, S. W.; Drakulic, S.; Deas, E.; Ouberai, M.; Aprile, F. A.; Arranz, R.; Ness, S.; Roodveldt, C.; Guilliams, T.; De-Genst, E. J.; Klenerman, D.; Wood, N. W.; Knowles, T. P.; Alfonso, C.; Rivas, G.; Abramov, A. Y.; Valpuesta, J. M.; Dobson, C. M.; Cremades, N. Structural Characterization of Toxic Oligomers That Are Kinetically Trapped During α-Synuclein Fibril Formation. *Proc. Natl. Acad. Sci. U. S. A.* **2015**, *112*, E1994−2003.

(16) Lorenzen, N.; Nielsen, S. B.; Buell, A. K.; Kaspersen, J. D.; Arosio, P.; Vad, B. S.; Paslawski, W.; Christiansen, G.; Valnickova-Hansen, Z.; Andreasen, M.; Enghild, J. J.; Pedersen, J. S.; Dobson, C. M.; Knowles, T. P.; Otzen, D. E. The Role of Stable α-Synuclein Oligomers in the Molecular Events Underlying Amyloid Formation. *J. Am. Chem. Soc.* **2014**, *136*, 3859−3868.

(17) Narhi, L.; Wood, S. J.; Steavenson, S.; Jiang, Y.; Wu, G. M.; Anafi, D.; Kaufman, S. A.; Martin, F.; Sitney, K.; Denis, P.; Louis, J. C.; Wypych, J.; Biere, A. L.; Citron, M. Both Familial Parkinson's Disease Mutations Accelerate Alpha-Synuclein Aggregation. *J. Biol. Chem.* **1999**, *274*, 9843−9846.

(18) Li, J.; Uversky, V. N.; Fink, A. L. Effect of Familial Parkinson's Disease Point Mutations A30P and A53T on the Structural Properties, Aggregation, and Fibrillation of Human Alpha-Synuclein. *Biochemistry* **2001**, *40*, 11604−11613.

(19) Fredenburg, R. A.; Rospigliosi, C.; Meray, R. K.; Kessler, J. C.; Lashuel, H. A.; Eliezer, D.; Lansbury, P. T. The Impact of the E46K Mutation on the Properties of Alpha-Synuclein in Its Monomeric and Oligomeric States. *Biochemistry* **2007**, *46*, 7107−1718.

(20) Tosatto, L.; Horrocks, M. H.; Dear, A. J.; Knowles, T. P.; Dalla Serra, M.; Cremades, N.; Dobson, C. M.; Klenerman, D. Single-Molecule FRET Studies on Alpha-Synuclein Oligomerization of Parkinson's Disease Genetically Related Mutants. *Sci. Rep.* **2015**, *5*, 16696.

(21) Flagmeier, P.; Meisl, G.; Vendruscolo, M.; Knowles, T. P.; Dobson, C. M.; Buell, A. K.; Galvagnion, C. Mutations Associated With Familial Parkinson's Disease Alter the Initiation and Amplification Steps of α-Synuclein Aggregation. *Proc. Natl. Acad. Sci. U. S. A.* **2016**, *113*, 10328−10333.

(22) Lashuel, H. A.; Petre, B. M.; Wall, J.; Simon, M.; Nowak, R. J.; Walz, T.; Lansbury, P. T. Alpha-Synuclein, Especially the Parkinson's Disease-Associated Mutants, Forms Pore-Like Annular and Tubular Protofibrils. *J. Mol. Biol.* **2002**, *322*, 1089−102.

(23) Sierecki, E.; Giles, N.; Bowden, Q.; Polinkovsky, M. E.; Steinbeck, J.; Arrioti, N.; Rahman, D.; Bhumkar, A.; Nicovich, P. R.; Ross, I.; Parton, R. G.; Böcking, T.; Gambin, Y. Nanomolar Oligomerization and Selective Co-Aggregation of α-Synuclein Pathogenic Mutants Revealed by Single-Molecule Fluorescence. *Sci. Rep.* **2016**, *6*, 37630.

(24) Chia, S.; Flagmeier, P.; Habchi, J.; Lattanzi, V.; Linse, S.; Dobson, C. M.; Knowles, T. P. J.; Vendruscolo, M. Monomeric and Fibrillar α-Synuclein Exert Opposite Effects on the Catalytic Cycle That Promotes the Proliferation of Aβ42 Aggregates. *Proc. Natl. Acad. Sci. U. S. A.* **2017**, *114* (30), 8005−8010.

(25) Yoshimoto, M.; Iwai, A.; Kang, D.; Otero, D. A.; Xia, Y.; Saitoh, T. NACP, the Precursor Protein of the Non-Amyloid Beta/A4 Protein (A Beta) Component of Alzheimer Disease Amyloid, Binds A Beta and Stimulates A Beta Aggregation. *Proc. Natl. Acad. Sci. U. S. A.* **1995**, *92*, 9141−9145.

(26) Jensen, P. H.; Hojrup, P.; Hager, H.; Nielsen, M. S.; Jacobsen, L.; Olesen, O. F.; Gliemann, J.; Jakes, R. Binding of Abeta to Alpha- and Beta-Synucleins: Identification of Segments in Alpha-Synuclein/NAC Precursor That Bind Abeta and NAC. *Biochem. J.* **1997**, *323*, 539−546.

(27) Mandal, P. K.; Pettegrew, J. W.; Masliah, E.; Hamilton, R. L.; Mandal, R. Interaction Between Abeta Peptide and Alpha Synuclein: Molecular Mechanisms in Overlapping Pathology of Alzheimer's and Parkinson's in Dementia With Lewy Body Disease. *Neurochem. Res.* **2006**, *31*, 1153−1162.

(28) Jensen, P. H.; Hager, H.; Nielsen, M. S.; Hojrup, P.; Gliemann, J.; Jakes, R. Alpha-Synuclein Binds to Tau and Stimulates the Protein Kinase A-Catalyzed Tau Phosphorylation of Serine Residues 262 and 356. *J. Biol. Chem.* **1999**, *274*, 25481−25489.

(29) Esposito, A.; Dohm, C. P.; Kermer, P.; Bähr, M.; Wouters, F. S. Alpha-Synuclein and Its Disease-Related Mutants Interact Differentially With the Microtubule Protein Tau and Associate With the Actin Cytoskeleton. *Neurobiol. Dis.* **2007**, *26*, 521−531.

(30) Qureshi, H. Y.; Paudel, H. K. Parkinsonian Neurotoxin 1-Methyl-4-Phenyl-1,2,3,6-Tetrahydropyridine (MPTP) and Alpha-Synuclein Mutations Promote Tau Protein Phosphorylation at Ser262 and Destabilize Microtubule Cytoskeleton *In Vitro. J. Biol. Chem.* **2011**, *286*, 5055−5068.

(31) Tsigelny, I. F.; Crews, L.; Desplats, P.; Shaked, G. M.; Sharikov, Y.; Mizuno, H.; Spencer, B.; Rockenstein, E.; Trejo, M.; Platoshyn, O.; Yuan, J. X.; Masliah, E. Mechanisms of Hybrid Oligomer Formation in the Pathogenesis of Combined Alzheimer's and Parkinson's Diseases. *PLoS One* **2008**, *3*, e3135.

(32) Jose, J. C.; Chatterjee, P.; Sengupta, N. Cross Dimerization of Amyloid-β and αSynuclein Proteins in Aqueous Environment: A Molecular Dynamics Simulations Study. *PLoS One* **2014**, *9*, e106883.

(33) Atsmon-Raz, Y.; Miller, Y. Non-Amyloid-β Component of Human α-Synuclein Oligomers Induces Formation of New Aβ

Oligomers: Insight Into the Mechanisms That Link Parkinson's and Alzheimer's Diseases. *ACS Chem. Neurosci.* **2016**, *7*, 46−55.

(34) De Ricco, R.; Valensin, D.; Dell'Acqua, S.; Casella, L.; Hureau, C.; Faller, P. Copper(I/II), α/β-Synuclein and Amyloid-β: Menage À Trois? *ChemBioChem* **2015**, *16*, 2319−2328.

(35) Nübling, G.; Bader, B.; Levin, J.; Hildebrandt, J.; Kretzschmar, H.; Giese, A. Synergistic Influence of Phosphorylation and Metal Ions on Tau Oligomer Formation and Coaggregation With α-Synuclein at the Single Molecule Level. *Mol. Neurodegener.* **2012**, *7*, 35.

(36) Sengupta, U.; Guerrero-Muñoz, M. J.; Castillo-Carranza, D. L.; Lasagna-Reeves, C. A.; Gerson, J. E.; Paulucci-Holthauzen, A. A.; Krishnamurthy, S.; Farhed, M.; Jackson, G. R.; Kayed, R. Pathological Interface Between Oligomeric Alpha-Synuclein and Tau in Synucleinopathies. *Biol. Psychiatry* **2015**, *78*, 672−83.

(37) Daniele, S.; Pietrobono, D.; Fusi, J.; Iofrida, C.; Chico, L.; Petrozzi, L.; Gerfo, A. L.; Baldacci, F.; Galetta, F.; Siciliano, G.; Bonuccelli, U.; Santoro, G.; Trincavelli, M. L.; Franzoni, F.; Martini, C. α-Synuclein Aggregates With β-Amyloid or Tau in Human Red Blood Cells: Correlation With Antioxidant Capability and Physical Exercise in Human Healthy Subjects. *Mol. Neurobiol.* **2018**, *55*, 2653−2675.

(38) Orte, A.; Clarke, R.; Klenerman, D. Single-Molecule Two-Colour Coincidence Detection To Probe Biomolecular Associations. *Biochem. Soc. Trans.* **2010**, *38*, 914−918.

(39) Iljina, M.; Garcia, G. A.; Dear, A. J.; Flint, J.; Narayan, P.; Michaels, T. C.; Dobson, C. M.; Frenkel, D.; Knowles, T. P.; Klenerman, D. Quantitative Analysis of Co-Oligomer Formation by Amyloid-Beta Peptide Isoforms. *Sci. Rep.* **2016**, *6*, 28658.

(40) Wille, H.; Drewes, G.; Biernat, J.; Mandelkow, E. M.; Mandelkow, E. Alzheimer-Like Paired Helical Filaments and Antiparallel Dimers Formed From Microtubule-Associated Protein Tau *In Vitro. J. Cell Biol.* **1992**, *118*, 573−584.

(41) Emmanouilidou, E.; Elenis, D.; Papasilekas, T.; Stranjalis, G.; Gerozissis, K.; Ioannou, P. C.; Vekrellis, K. Assessment of α-Synuclein Secretion in Mouse and Human Brain Parenchyma. *PLoS One* **2011**, *6*, e22225.

(42) Tong, J.; Wong, H.; Guttman, M.; Ang, L. C.; Forno, L. S.; Shimadzu, M.; Rajput, A. H.; Muenter, M. D.; Kish, S. J.; Hornykiewicz, O.; Furukawa, Y. Brain Alpha-Synuclein Accumulation in Multiple System Atrophy, Parkinson's Disease and Progressive Supranuclear Palsy: A Comparative Investigation. *Brain* **2010**, *133*, 172−188.

(43) Mollenhauer, B.; Locascio, J. J.; Schulz-Schaeffer, W.; Sixel-Döring, F.; Trenkwalder, C.; Schlossmacher, M. G. α-Synuclein and Tau Concentrations in Cerebrospinal Fluid of Patients Presenting With Parkinsonism: A Cohort Study. *Lancet Neurol.* **2011**, *10*, 230−240.

(44) Apetri, M. M.; Maiti, N. C.; Zagorski, M. G.; Carey, P. R.; Anderson, V. E. Secondary Structure of Alpha-Synuclein Oligomers: Characterization by Raman and Atomic Force Microscopy. *J. Mol. Biol.* **2006**, *355*, 63−71.

(45) Wood, S. J.; Wypych, J.; Steavenson, S.; Louis, J. C.; Citron, M.; Biere, A. L. Alpha-Synuclein Fibrillogenesis Is Nucleation-Dependent. Implications for the Pathogenesis of Parkinson's Disease. *J. Biol. Chem.* **1999**, *274*, 19509−19512.

(46) Barghorn, S.; Biernat, J.; Mandelkow, E. Purification of Recombinant Tau Protein and Preparation of Alzheimer-Paired Helical Filaments *In Vitro. Methods Mol. Biol.* **2005**, *299*, 35−51.

(47) Jeganathan, S.; von Bergen, M.; Mandelkow, E. M.; Mandelkow, E. The Natively Unfolded Character of Tau and Its Aggregation to Alzheimer-Like Paired Helical Filaments. *Biochemistry* **2008**, *47*, 10526−10539.

(48) Horrocks, M. H.; Tosatto, L.; Dear, A. J.; Garcia, G. A.; Iljina, M.; Cremades, N.; Dalla Serra, M.; Knowles, T. P.; Dobson, C. M.; Klenerman, D. Fast Flow Microfluidics and Single-Molecule Fluorescence for the Rapid Characterization of α-Synuclein Oligomers. *Anal. Chem.* **2015**, *87*, 8818−8826.

(49) Iljina, M.; Garcia, G. A.; Horrocks, M. H.; Tosatto, L.; Choi, M. L.; Ganzinger, K. A.; Abramov, A. Y.; Gandhi, S.; Wood, N. W.;

Cremades, N.; Dobson, C. M.; Knowles, T. P.; Klenerman, D. Kinetic Model of the Aggregation of Alpha-Synuclein Provides Insights Into Prion-Like Spreading. *Proc. Natl. Acad. Sci. U. S. A.* **2016**, *113*, E1206−1215.

(50) Lee, H. J.; Bae, E. J.; Lee, S. J. Extracellular Alpha-Synuclein - A Novel and Crucial Factor in Lewy Body Diseases. *Nat. Rev. Neurol.* **2014**, *10*, 92−98.

(51) Himmler, A.; Drechsel, D.; Kirschner, M. W.; Martin, D. W. Tau Consists of a Set of Proteins With Repeated C-Terminal Microtubule-Binding Domains and Variable N-Terminal Domains. *Mol. Cell. Biol.* **1989**, *9*, 1381−1388.

(52) Atwood, C. S.; Martins, R. N.; Smith, M. A.; Perry, G. Senile Plaque Composition and Posttranslational Modification of Amyloid-Beta Peptide and Associated Proteins. *Peptides* **2002**, *23*, 1343−1350.

(53) Wright, C. F.; Teichmann, S. A.; Clarke, J.; Dobson, C. M. The Importance of Sequence Diversity in the Aggregation and Evolution of Proteins. *Nature* **2005**, *438*, 878−881.

(54) Singleton, A. B.; Farrer, M.; Johnson, J.; Singleton, A.; Hague, S.; Kachergus, J.; Hulihan, M.; Peuralinna, T.; Dutra, A.; Nussbaum, R.; Lincoln, S.; Crawley, A.; Hanson, M.; Maraganore, D.; Adler, C.; Cookson, M. R.; Muenter, M.; Baptista, M.; Miller, D.; Blancato, J.; et al. Alpha-Synuclein Locus Triplication Causes Parkinson's Disease. *Science* **2003**, *302* (5646), 841.

(55) Ahn, T. B.; Kim, S. Y.; Kim, J. Y.; Park, S. S.; Lee, D. S.; Min, H. J.; Kim, Y. K.; Kim, S. E.; Kim, J. M.; Kim, H. J.; Cho, J.; Jeon, B. S. Alpha-Synuclein Gene Duplication Is Present in Sporadic Parkinson Disease. *Neurology* **2008**, *70*, 43−49.

(56) Ibáñez, P.; Bonnet, A. M.; Débarges, B.; Lohmann, E.; Tison, F.; Pollak, P.; Agid, Y.; Dürr, A.; Brice, A. Causal Relation Between Alpha-Synuclein Gene Duplication and Familial Parkinson's Disease. *Lancet* **2004**, *364*, 1169−1171.

(57) Galvagnion, C.; Brown, J. W.; Ouberai, M. M.; Flagmeier, P.; Vendruscolo, M.; Buell, A. K.; Sparr, E.; Dobson, C. M. Chemical Properties of Lipids Strongly Affect the Kinetics of the Membrane-Induced Aggregation of α-Synuclein. *Proc. Natl. Acad. Sci. U. S. A.* **2016**, *113*, 7065−7070.

(58) Mehta, P. D.; Pirttilä, T.; Mehta, S. P.; Sersen, E. A.; Aisen, P. S.; Wisniewski, H. M. Plasma and Cerebrospinal Fluid Levels of Amyloid Beta Proteins 1−40 and 1−42 in Alzheimer Disease. *Arch. Neurol.* **2000**, *57*, 100−105.

(59) Galvagnion, C.; Buell, A. K.; Meisl, G.; Michaels, T. C.; Vendruscolo, M.; Knowles, T. P.; Dobson, C. M. Lipid Vesicles Trigger α-Synuclein Aggregation by Stimulating Primary Nucleation. *Nat. Chem. Biol.* **2015**, *11*, 229−234.

(60) Demuro, A.; Mina, E.; Kayed, R.; Milton, S. C.; Parker, I.; Glabe, C. G. Calcium Dysregulation and Membrane Disruption as a Ubiquitous Neurotoxic Mechanism of Soluble Amyloid Oligomers. *J. Biol. Chem.* **2005**, *280*, 17294−17300.

(61) Flagmeier, P.; De, S.; Wirthensohn, D. C.; Lee, S. F.; Vincke, C.; Muyldermans, S.; Knowles, T. P. J.; Gandhi, S.; Dobson, C. M.; Klenerman, D. Ultrasensitive Measurement of Ca(2+) Influx Into Lipid Vesicles Induced by Protein Aggregates. *Angew. Chem., Int. Ed.* **2017**, *56*, 7750−7754.

(62) Narayan, P.; Orte, A.; Clarke, R. W.; Bolognesi, B.; Hook, S.; Ganzinger, K. A.; Meehan, S.; Wilson, M. R.; Dobson, C. M.; Klenerman, D. The Extracellular Chaperone Clusterin Sequesters Oligomeric Forms of the Amyloid-β(1−40) Peptide. *Nat. Struct. Mol. Biol.* **2012**, *19*, 79−83.

(63) Kiely, A.; Asi, Y.; Kara, E.; Limousin, P.; Ling, H.; Lewis, P.; Proukakis, C.; Quinn, N.; Lees, A.; Hardy, J.; Revesz, T.; Houlden, H.; Holton, J. Synucleinopathy With a G51D α-Synuclein Mutation: A Neuropathological and Genetic Study. *Neuropathol. Appl. Neurobiol.* **2013**, *39*, 39−40.

(64) Pasanen, P.; Myllykangas, L.; Siitonen, M.; Raunio, A.; Kaakkola, S.; Lyytinen, J.; Tienari, P. J.; Pöyhönen, M.; Paetau, A. Novel α-Synuclein Mutation A53E Associated With Atypical Multiple System Atrophy and Parkinson's Disease-Type Pathology. *Neurobiol. Aging* **2014**, *35*, 2180.

(65) Kellie, J. F.; Higgs, R. E.; Ryder, J. W.; Major, A.; Beach, T. G.; Adler, C. H.; Merchant, K.; Knierman, M. D. Quantitative Measurement of Intact Alpha-Synuclein Proteoforms From Post-Mortem Control and Parkinson's Disease Brain Tissue by Intact Protein Mass Spectrometry. *Sci. Rep.* **2015**, *4*, 5797.

(66) Takami, M.; Nagashima, Y.; Sano, Y.; Ishihara, S.; Morishima-Kawashima, M.; Funamoto, S.; Ihara, Y. Gamma-Secretase: Successive Tripeptide and Tetrapeptide Release From the Transmembrane Domain of Beta-Carboxyl Terminal Fragment. *J. Neurosci.* **2009**, *29*, 13042−13052.

(67) Guerrero, C.; Tagwerker, C.; Kaiser, P.; Huang, L. An Integrated Mass Spectrometry-Based Proteomic Approach: Quantitative Analysis of Tandem Affinity-Purified *In Vivo* Cross-Linked Protein Complexes (QTAX) to Decipher the 26 S Proteasome-Interacting Network. *Mol. Cell. Proteomics* **2006**, *5*, 366−378.

(68) Hoyer, W.; Antony, T.; Cherny, D.; Heim, G.; Jovin, T.; Subramaniam, V. Dependence of Alpha-Synuclein Aggregate Morphology on Solution Conditions. *J. Mol. Biol.* **2002**, *322*, 383−393.

(69) Shammas, S. L.; Garcia, G. A.; Kumar, S.; Kjaergaard, M.; Horrocks, M. H.; Shivji, N.; Mandelkow, E.; Knowles, T. P.; Klenerman, D.; Mandelkow, E. A Mechanistic Model of Tau Amyloid Aggregation Based on Direct Observation of Oligomers. *Nat. Commun.* **2015**, *6*, 7025.

(70) Teplow, D. B. Preparation of Amyloid Beta-Protein for Structural and Functional Studies. *Methods Enzymol.* **2006**, *413*, 20−33.

(71) Horrocks, M. H.; Lee, S. F.; Gandhi, S.; Magdalinou, N. K.; Chen, S. W.; Devine, M. J.; Tosatto, L.; Kjaergaard, M.; Beckwith, J. S.; Zetterberg, H.; Iljina, M.; Cremades, N.; Dobson, C. M.; Wood, N. W.; Klenerman, D. Single-Molecule Imaging of Individual Amyloid Protein Aggregates in Human Biofluids. *ACS Chem. Neurosci.* **2016**, *7*, 399−406.

(72) Ying, L.; Wallace, M.; Balasubramanian, S.; Klenerman, D. Ratiometric Analysis of Single-Molecule Fluorescence Resonance Energy Transfer Using Logical Combinations of Threshold Criteria: A Study of 12-Mer DNA. *J. Phys. Chem. B* **2000**, *104*, 5171−5178.

(73) Clarke, R.; Orte, A.; Klenerman, D. Optimized Threshold Selection for Single-Molecule Two-Color Fluorescence Coincidence Spectroscopy. *Anal. Chem.* **2007**, *79*, 2771−2777.

(74) Efron, B. Bootstrap Methods: Another Look at the Jackknife. *Ann. Stat.* **1979**, *7*, 1−26.

(75) Rao, J. N. K.; Wu, C. F. J. Resampling Inference With Complex Survey Data. *J. Am. Stat. Assoc.* **1988**, *83*, 231−241.

(76) Bickel, P. J.; Götze, F.; van Zwet, W. R. Resampling Fewer Than *n* Observations: Gains, Losses, and Remedies for Losses. *Stat. Sin.* **1997**, *7*, 1−31.

(77) Choi, W.; Zibaee, S.; Jakes, R.; Serpell, L. C.; Davletov, B.; Crowther, R. A.; Goedert, M. Mutation E46K Increases Phospholipid Binding and Assembly Into Filaments of Human Alpha-Synuclein. *FEBS Lett.* **2004**, *576*, 363−368.

(78) Middleton, E.; Rhoades, E. Effects of Curvature and Composition on Alpha-Synuclein Binding to Lipid Vesicles. *Biophys. J.* **2010**, *99*, 2279−2288.